Research on Surface Modification of Screen Printing Electronics

Ye Tian
Beijing Institute of Graphic Communication https://orcid.org/0000-0002-6805-0982
Yan Li (137330424@qq.com)
Beijing University of Aeronautics and Astronautics https://orcid.org/0000-0002-6273-1218
Ying-Cai Yuan
beijing yinshua xueyuan
Lin Zhao
Shougang co.,Ltd
Gao-Shen He
beijing yinshua xueyuan
Tuo-Kai Peng
Beijing University of Chemical Technology
Jian-Lin Xu
beijing yinshua xueyuan

Original Article

Keywords: Adhesion mechanism, Printed electronics, Modification technology, Liquid bridge, Fluent

Posted Date: September 30th, 2021

DOI: https://doi.org/10.21203/rs.3.rs-936681/v1

Title page

Research on Surface Modification of Screen Printing Electronics

Ye Tian, born in 1995, is currently an engineer at *Beijing Key Laboratory of Digitization Printing Equipment, Beijing Institute of Printing, Beijing*. He received his master degree from *Beijing Institute of Graphic Communication, China*, in 2021. His research interests are screen printing electronics.
E-mail: 787706522@qq.com

Yan Li, born in 1965, is currently an professor at *Beijing Institute of Graphic Communication, China*. She received his master degree from *Beijing University of Aeronautics and Astronautics, China*, in 1999. Her research interests are flexible electronic technology and equipment, printing machinery innovation design, Triz theory and application.
Tel: +86-13621060612 E-mail: 137330424@qq.com

Ying-Cai Yuan, born in 1973, is currently an associate professor at *Beijing Institute of Graphic Communication, China.* He received his PhD degree from *Central South University, China*, in 2011. His research interests are flexible electronic technology and equipment and printing machinery innovation design.
E-mail: yuan_yc@bigc.edu.cn

Lin Zhao, born in 1964, is currently a professor at *Shougang CO.,Ltd, China*. He received his PhD degree from *Northeastern University, China,* in 1997. His research interests include mechanics engineering, metal material and automatic control.
E-mail: 13522592591@163.com

Gao-Shen He, born in 1985, is currently an engineer at *Beijing Key Laboratory of Digitization Printing Equipment, Beijing Institute of Printing, Beijing*. He received his master degree from *Beijing Institute of Graphic Communication, China*, in 2021. His research interests include Bio-3D printing, digital printing, medical robotics.
E-mail: 591526804@qq.com

Tuo-Kai Peng, born in 1993, is currently a master candidate at *Beijing Advanced Innovation Center for Soft Matter Science and Engineerin*g, Beijing University of Chemical Technology, China.
E-mail: PengTuokai@163.com

Jian-Lin Xu, born in 1998, is currently a master candidate at *Beijing Key Laboratory of Digitization Printing Equipment, Beijing Institute of Printing, Beijing Institute of Graphic Communication, China.* His research interests are screen printing electronics.
E-mail: 1770170376@qq.com

Corresponding author：Li Yan　E-mail：137330424@qq.com

ORIGINAL ARTICLE

Research on Surface Modification of Screen Printing Electronic

Ye Tian[1,2,3] • Yan Li[1,2,3] • Ying-Cai Yuan[1,2] • Lin Zhao[4] • Gao-Shen He[1,2,3] • Tuo-Kai Peng[5] • Jian-lin Xu[1,2,3]

Abstract: Printing electronic components by screen printing with its excellent printing quality, high efficiency, and green environmental protection have broad application prospects in additive manufacturing. However, efficiency and quality of printing were decreased as conductive-ink blocking screen in the actual process of printing. Thus, it is pivotal that exploring factors of adhesion from the interaction of conductive-ink and screen. Herein, the functional relationship between adhesion and factors of adhesion and influence trend of adhesion on ink residue was obtained via the establishment of liquid-bridge adhesion model between two plates according to screen printing ink transfer process, solid-liquid wetting theory, and adhesion mechanism, which was verified by software Fluent. In order to justify the accuracy of the model and simulation, the adhesion and ink residue were tested on the surface-modified glass sheet as the result that the model and simulation were consistent with the experimental record. It was demonstrated that solid-liquid contact angle, tensile distance, and liquid volume are the main factors affecting the change of solid-liquid adhesion. With the increase of tensile distance and contact angle, the adhesion force decreases, which causes the decline of the residual amount of liquid on the solid surface. By means of screen modification, the adhesion between conductive-ink and screen can be reduced, as meanwhile the efficiency and quality of printed products can be improved.

Keywords: Adhesion mechanism • Printed electronics • Modification technology • Liquid bridge • Fluent

✉ Ye Tian
787706522@qq.com

[1] Beijing Key Laboratory of Digitization Printing Equipment, Beijing Institute of Graphic Communication, Beijing 102600, China

[2] Research Center of Printing Equipment of Beijing Universities, Beijing Institute of Graphic Communication, Beijing 102600, China

[3] Beijing Engineering Research Center of Printed Electronics, Beijing 102600, China

[4] Beijing Shougang Co., Ltd., Beijing 102206, China

[5] Beijing Advanced Innovation Center for Soft Matter Science and Engineering, Beijing University of Chemical Technology, Beijing 100029, China

1 Introduction

Printed electronics is an additive manufacturing technology that uses traditional printing methods to manufacture electronic components and circuits and realizes the integration of printing and electronics[1]. Advantages are flexibility, large format, and low cost [2–5]. Printing electronic components by screen printing (hereinafter referred to as screen printing electronics) has gradually become the most widely used and mature production process in the field of printing electronics with the advantages of high ink layer thickness, high conductivity, low cost, and environmental protection[6-11].

In a printing process of screen printing electronics, the conductive ink is squeezed through the screen image and text area under the horizontal movement of the scraper and spreads on the printing substrate to form a print. The schematic diagram of ink transfer is shown in Figure 1. Printing quality requires good use performance and high precision [12-16]. The key to high-quality printing is to establish a printing technology with high resolution and Ink Transferring Rate. Lorenz [17] pointed out that by printing silicon solar cells by screen printing, the electrode width was reduced from 120μm to 28μm. The general method to improve printing resolution is to select the screen mesh with a large mesh and small aperture. However, in printing production, the smaller aperture will cause the conductive ink to block the screen frequently, as shown in Figure 2, thus the amount of ink transferred to the substrate (hereinafter referred to as Ink Transferring Rate), the thickness of ink layer was reduced, the conductivity of printed lines became worse either [18-20]. To solve the problem of Ink Transferring Rate reduction, scholars at home and abroad have increased the Ink Transferring Rate

by changing the screen structure [20,21], the rheological properties of conductive ink [20,22-24], printing process parameters [25,26], etc., but there are some drawbacks. Taking the knotless net screen printing stencil as an example, this structure reduces the durability of the screen while increasing the ink transfer rate, and the high plate-making cost increases the printing cost.

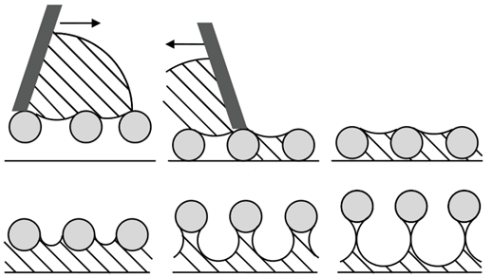

Figure 1 Schematic diagram of ink transfer

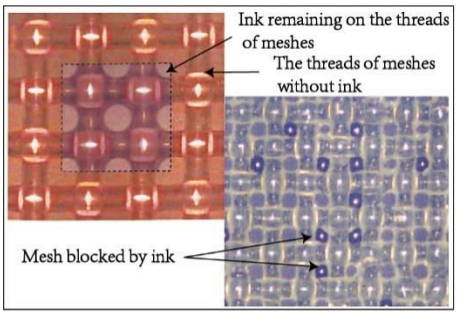

Figure 2 Screen printing blocked by conductive ink

The mechanism of ink transfer in printing electronics was studied. Liu et al. explored the mechanism of ink transfer in screen printing and thought that increasing the dynamic pressure in the wedge-shaped area could ensure enough ink drop on the substrate [27]; Lee et al. improved the ink transferring rate and printing stability by exploring the process parameters of gravure printing [28]; Chu analyzed the influence of ink flow and ink transferring rate on the rotation speed of two ink rollers when they roll against each other, ink rollers diameter and ink layer thickness before two ink rollers' contacting [29]. Kapur established a mathematical model of ink transfer in screen printing and proposed that ink surface energy is the key factor affecting ink transfer [30]. It can be seen that the research on ink transfer mechanism is mostly aimed at the influence of printing process parameters, and few scholars have explored the influent of adhesion between the ink and the screen in screen printing electronics. Achieving controllable adhesion is an effective way to solve ink-blocking mesh in the electronic field of screen printing and improve the ink transferring rate. In order to regulate the surface adhesion independently according to the performance requirements, domestic and foreign researchers defined the pulling force needed to separate two contact objects as adhesion, and used adhesion as an index to measure the size of adhesion [31], and put forward a variety of methods [32] to regulate the surface adhesion from the perspectives of changing the contact area [33-37] and changing the surface energy [38-41], which is mainly divided into "reshaping" and "modification." Wu et al. [42] prepared nano-convex-patterned polyimide surface and nano-concave patterned polyimide surface, which effectively reduced the adhesion on the surface of the samples. Shivaprakash et al. [43] prepared nano-silica particles on silicon wafers. It is found that nanoparticles can reduce the adhesion of silicon wafer surface. Qing et al. [44] prepared a titanium diboride coating on a silicon wafer, the surface adhesion with this coating decreased by about 75% compared with that on the bare silicon surface. Liang [45] and others reported a Fluorine-containing onion carbon organic film, which reduced the surface adhesion by about 90% compared with Trifluoroacetic acid.

Based on the fact that modification has become the most economical and effective means to regulate the adhesion between conductive ink and screen printing plate, the summation that reduction of surface energy and contact area can reduce adhesion was verified by a considerable number of experiments, while the clear conclusion about the functional relationship between surface energy and adhesion has not been obtained yet. Hence, we constructed an adhesion model of conductive ink to obtain the functional relationship between adhesion and surface energy (characterized by contact angle) and contact area, as and established a simulation analysis model to verify the conclusion of the adhesion model and acquired the influence trend of adhesion on ink residue. It is indicated that the adhesion model and simulation analysis model are consistent with the practical result through the liquid bridge tensile fracture experiment.

2 Model of Liquid Bridge Adhesion Between Two Plates under Gravity-free Condition

2.1 Adhesion Mechanism in Surface Modification

When the liquid drops are placed on a smooth solid surface, the liquid drops spread on the solid surface, and the solid-vapor interface is replaced by the solid-liquid interface, and the liquid-vapor interface is enlarged. Under isothermal and isobaric conditions, the change of surface energy per unit area before and after the solid surface is wetted, that is, the change of Gibbs free energy function, is

shown in Eq. (1). Shown as Eq. (2) for spreading parameter S, which means the change of surface energy per unit area before and after surface wetting. Among γ_{sl}, γ_{sv}, γ_{lv}, they are "solid-liquid", "solid-vapor" and "liquid-vapor" interfacial tensions. According to the second law of thermodynamics, When $S \geq 0$, the droplets completely wet the solid surface and spontaneously spread on the solid surface. When $S < 0$, droplets partially wet the solid surface and keep an equilibrium shape in spherical form [46].

$$\Delta G = \gamma_{sl} + \gamma_{lv} - \gamma_{sv}, \tag{1}$$

$$S = -\Delta G / A = \gamma_{sv} - (\gamma_{sl} + \gamma_{lv}) \tag{2}$$

When $S < 0$, the droplets spread on the solid surface and reach equilibrium, the angle formed by the vapor-liquid interface and the solid-liquid interface at the intersection of vapor-liquid-solid three phases is defined as the contact angle θ, the spreading of droplets on the solid surface is shown in Figure 3. The surface energy of solid γ_{sv} is generally difficult to measure. Therefore, contact angles θ is used to characterize the wetting difficulty of the solid surface. In 1805, aimed at partial wetting, Thomas Young quantitatively analyzed the relationship between solid surface free energy and contact angle [47], and Young's equation is shown in Eq. (3).

$$\cos\theta = \frac{\gamma_{sv} - \gamma_{sl}}{\gamma_{lv}}, \tag{3}$$

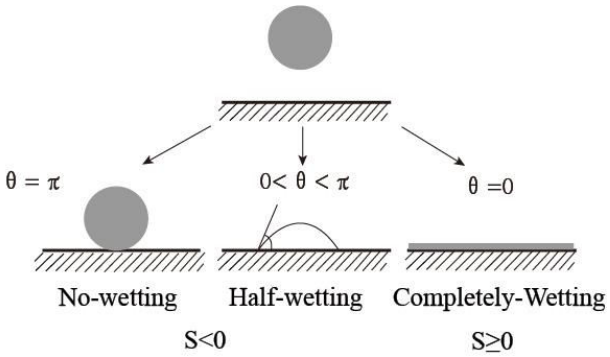

Figure 3 Spreading of liquid droplets on a solid surface

Under isothermal and isobaric conditions, when the liquid adheres to the solid surface per unit area, as shown in Figure 4, the surface tension force is γ_{sl}, it is separated into two independent phases by an external force, the surface tension force is γ_{lv} and γ_{sv}. In this separation process, the work done by the external force is called adhesion work W_a. It is shown as the Eq. (4) for the expression.

$$W_a = \gamma_{lv} + \gamma_{sv} - \gamma_{sl}, \tag{4}$$

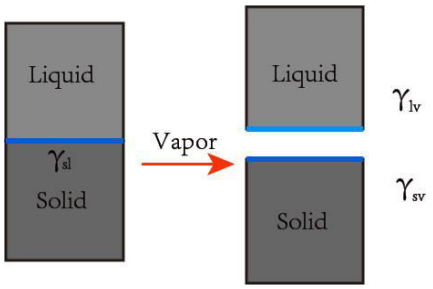

Figure 4 Schematic diagram of the two-phase separation

Combined with Young's equation Dupre to simplified Eq. (3), and the relationship between adhesion work and contact angle is shown in Eq. (5) [48].

$$W_a = \gamma_{lv}(1 + \cos\theta), \tag{5}$$

From the point of view of energy, the research on the modification of screen printing electronics is considered. If the properties of fixed conductive ink do not change, the wettability of conductive ink on the screen can be affected by changing the surface energy of the screen so as to achieve the purpose of changing the adhesion ability between solid and liquid, and finally solve the problem of ink adhering to the screen.

2.2 Force Analysis of Droplets

Generally, when the capillary length is larger than the characteristic scale of liquid, the influence of gravity can be ignored [49], and the capillary length formula is defined as:

$$l_c = \sqrt{\frac{\gamma}{\rho g}}, \tag{6}$$

Where γ is the liquid surface tension, N/m, ρ is liquid density, kg/m^3, g is the acceleration of gravity, m/s^2.

Definition is made as following: the surface tension of conductive silver ink 0.03 N/m, the density is 1950 kg/m^3, capillary length is 1.253mm, this length is taken as the ink droplet diameter, the volume is 1.03μL. In this volume, the influence of surface tension on ink droplets is greater than that of gravity, and the influence of gravity is negligible.

2.3 Model of Liquid Bridge Adhesion Between Two Plates

According to the schematic diagram of ink transfer, it is necessary to overcome the adhesion between ink and screen to reduce the residual amount of ink on screen printing. It is very important to build a solid-liquid adhesion and separation model to research modification of screen printing electronics. Modeling the tensile fracture process of a single screen thread and conductive ink in the screen, when the geometric radius of a single screen thread is extended wirelessly, the cylindrical screen thread is simplified as a flat plate, and the model is simplified as the tensile fracture process between conductive ink and two flat plates. The tensile fracture model based on the liquid bridge between two plates is simple and versatile, which provides reference experience for establishing a more reasonable model.

It is assumed that the contact angle of ink and upper and lower plates are the same θ, in addition, in the process of stretching, the influence of gravity of the liquid phase is neglected, in the process of stretching and breaking of the liquid phase, the liquid phase will not evaporate or condense, and the volume is conserved, the two plates are rigid. The schematic diagram of the liquid bridge between two plates is shown in Figure 5. The adhesive force F acting on the plane is mainly affected by capillary force, which consists of the following two parts:

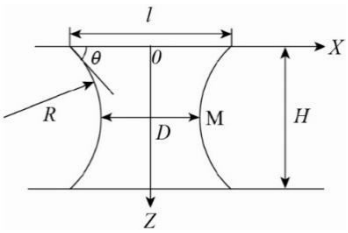

Figure5 Schematic diagram of liquid bridge between two plates

(1) Adhesion caused by the pressure difference between inside and outside the meniscus Δp.

(2) Vertical component of surface tension in the tangential direction of the liquid meniscus.

Therefore:

$$F_1 = \pi\left(\frac{l}{2}\right)^2 \Delta p_1 + \pi l \cdot \gamma \cdot \sin\theta, \tag{7}$$

In Eq. (7), l is the diameter of the contact part between the liquid phase and two plates m. When the liquid bridge is stable, the Young-Laplace equation is satisfied at the liquid phase contour point M, as shown in Eq. (8).

$$\Delta p_1 = \gamma\left(\frac{1}{r_1} + \frac{1}{r_2}\right), \tag{8}$$

According to the Young-Laplace equation, in general, in order to obtain the expression of liquid bridge capillary force and the appearance model of the liquid bridge, the meniscus is assumed to be a circular arc, so r_1 and r_2 in the differential equation can be expressed as the two main radii of curvature of the liquid-vapor two-phase interface in liquid bridge:

$$r_1 = R, \tag{9}$$

$$r_2 = -\frac{D}{2}, \tag{10}$$

=

The following relations can be obtained from the basic assumptions, as shown in Eq. (11) and Eq. (12). In which H is the height of the liquid bridge and D is the diameter of the necking part of the liquid bridge.

$$R = \frac{H}{2\cos\theta}, \tag{11}$$

$$l = D + 2R\left(1 - \sin\theta\right), \tag{12}$$

The volume of the liquid bridge is approximated as a cylindrical volume, and the diameter l of the cylinder takes the intermediate value between the wetting diameter of the liquid bridge and the diameter D at the neck of the liquid bridge so that the approximate volume expression of the liquid bridge can be obtained as Eq. (13).

$$V = \pi\left(\frac{D+l}{4}\right)^2 H, \tag{13}$$

l and D can be obtained from the joint Eqs. (11)-(13). The expression, as shown type Eqs. (14), (15).

$$l = \sqrt{\frac{4V}{\pi H}} + \frac{H\left(1-\sin\theta\right)}{2\cos\theta}, \tag{14}$$

$$D = \sqrt{\frac{4V}{\pi H}} - \frac{H\left(1-\sin\theta\right)}{2\cos\theta}, \tag{15}$$

Therefore, according to the Young-Laplace equation, the pressure difference between inside and outside the liquid-vapor phase can be obtained, as shown in Eq. (16).

$$\Delta p_1 = \gamma\left(\frac{2\cos\theta}{H} - \frac{2}{\sqrt{\frac{4V}{\pi H}} - \frac{H\left(1-\sin\theta\right)}{2\cos\theta}}\right), \tag{16}$$

To sum up, the expression of liquid bridge adhesion between two plates is shown in Eq. (17).

$$F1=\pi\left(\frac{\sqrt{\frac{4V}{\pi H}}+\frac{H\left(1-\sin\theta\right)}{2\cos\theta}}{2}\right)^2\gamma\left(\frac{2\cos\theta}{H}-\frac{2}{\sqrt{\frac{4V}{\pi H}}-\frac{H\left(1-\sin\theta\right)}{2\cos\theta}}\right)+\pi\left(\sqrt{\frac{4V}{\pi H}}+\frac{H\left(1-\sin\theta\right)}{2\cos\theta}\right)\gamma\sin\theta \tag{17}$$

From the above expression, it can be seen that the liquid bridge adhesion between two plates is related to the liquid volume, solid-liquid contact angle and stretching distance.

2.3 Analysis of Calculation Results of Liquid Bridge Adhesion Model Between Two Plates

In the theoretical derivation of the liquid bridge model between two plates, when the upper plate moves upwards, it is assumed that the solid contact angle between the liquid phase and the lower plate does not change. The volume of the conductive ink is expressed by Eq. (13). Under the condition of the same liquid bridge volume calculated by Eq. (17), the change value of adhesion force with stretching distance under different contact angles is shown in Table 1. According to the model data in Table 1, draw a graph of changes in adhesion and stretching distance, as shown in Figure 6. It can be seen from the figure that (1) the adhesion decreases with the increase of stretching distance, and when the stretching distance reaches 1 mm, the adhesion tends to 0 N, indicating that the liquid bridge has broken at this time. (2) At the same stretching distance, the larger the contact angle is, the smaller the corresponding adhesion force is, that is, with the increase of contact angle, the more easily the liquid bridge breaks.

Meanwhile, according to Eq. (17), under the premise that the contact angle is constant at 40°, the changed value of the adhesion force of the liquid bridge with different liquid bridge volumes versus the stretching distance is shown in Table 2 (the maximum volume is not more than 1 μL). According to Table2, Draw a graph of the change of adhesion force with stretching distance, as shown in Figure 7. It can be seen from Figure 7 that under the same stretching distance, the smaller the volume of the liquid bridge, the smaller the adhesive force, which is caused by the decrease of liquid volume and the area of auxiliary development on the solid surface.

Table 1 Theoretical value of liquid bridge adhesion under different contact angles

Stretching distance H (mm)	Adhesion force F (x10^{-4}N)							
	10°	20°	30°	40°	50°	60°	70°	80°
0.1	59.34	56.92	52.77	47.02	39.84	31.44	22.10	12.07
0.2	14.88	14.43	13.53	12.21	10.52	8.51	6.24	3.77
0.3	6.59	6.48	6.18	5.67	4.99	4.14	3.18	2.11
0.4	3.63	3.65	3.55	3.34	3.00	2.57	2.05	1.47
0.5	2.21	2.30	2.31	2.22	2.05	1.81	1.50	1.15
0.6	1.40	1.53	1.59	1.59	1.51	1.37	1.18	0.95
0.7	0.85	1.03	1.14	1.19	1.16	1.10	0.97	0.82
0.8	0.43	0.67	0.82	0.90	0.93	0.90	0.84	0.73
0.9	0.09	0.37	0.57	0.69	0.75	0.76	0.73	0.66
1.0	0	0.12	0.36	0.52	0.61	0.65	0.65	0.60

Table 2 Theoretical value of liquid bridge adhesion force under different liquid bridge volume

Stretching distance H (mm)	Adhesion force F (x10^{-4}N)				
	Liquid bridge volume(1v=1 μL)				
	0.2v	0.4v	0.6v	0.8v	1v
0.1	9.66	19.12	28.44	37.73	47.02
0.2	2.60	5.04	7.45	9.84	12.21
0.3	1.24	2.38	3.49	4.59	5.67
0.4	0.73	1.41	2.06	2.70	3.34
0.5	0.46	0.93	1.37	1.80	2.22
0.6	0.28	0.64	0.97	1.28	1.59
0.7	0.14	0.44	0.70	0.95	1.19
0.8	0	0.29	0.51	0.71	0.90
0.9	0	0.15	0.35	0.53	0.69
1.0	0	0	0.21	0.37	0.52

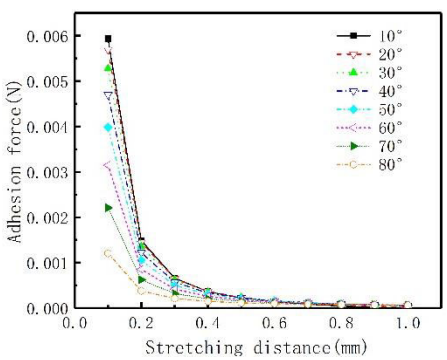

Figure 6 Variation curve of adhesion force with stretching distance under different contact angles

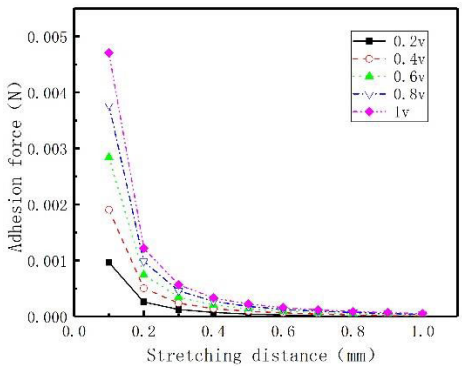

Figure 7 Variation curve of adhesion force of different liquid bridge volumes with stretching distance (40°)

3 Simulation Study on Tensile Fracture Process of Liquid Bridge

3.1 Model Building and Grid Division

3.1.1 Model Establishment

The VOF method is used to simulate the tensile fracture of the liquid bridge between two plates by CFD, and the ICEM software in Ansys Workbench is used to model the tensile fracture process of the liquid bridge between two plates in two dimensions. The calculation domain of 5mm x 10mm in the x-y plane is established, and the software in Z-axis direction is defined as unit length, as shown in Figure 8. The length of the upper plate is L_1=2mm, and the width is L_2=0.5mm.

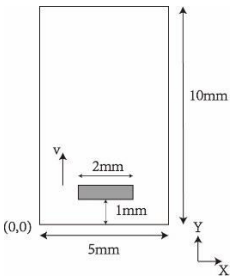

Figure 8 Two-plane two-dimensional model

3.1.2 Grid Division of Two-dimensional Model between Two Flat Plates

Based on modeling in the previous step, the fluid domain is divided into the fluid region and fluid-move region. The fluid-move area moves upward with the upper plate at a constant speed, and the position of the upper plate changes constantly, so the grid is dynamically processed. The whole model is divided into grids in a mixed grid mode, which has the advantage of improving grid quality, reducing the computation and saving time. The area division is shown as Figure 9 (a). The hybrid grid is composed of an unstructured grid and a structured grid, in which the structured grid is a quadrilateral grid, which is defined as the upward moving fluid-move region. As shown in Figure 9 (b), the minimum side length of the quadrilateral grid is $5.78e^{-5}$ m, and the maximum side length of the quadrilateral grid is $5.83e^{-5}$ m. Unstructured mesh is composed of triangular meshes, which are defined as a constant fluid region, as shown in Figure 9 (c). The minimum side length is $3.08417e^{-5}$ m, the maximum side length is $8.6211e^{-5}$ m, and the number of corresponding grids in the simulation domain is 41,600.

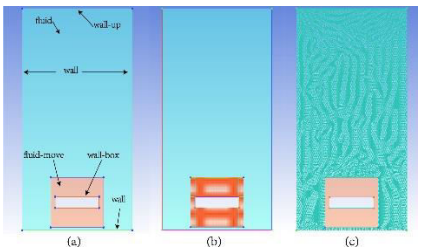

Figure 9 Grid division of ICEM two-dimensional model

3.2 Numerical Simulation Parameter Setting

The ANSYS FLUENT 17.0 computational fluid dynamics software is used for numerical simulation, and the basic parameters used in the simulation experiment are shown in Table 3.

Table 3 Basic simulation parameters

Model Parameter	Numerical Value
Contact angle of upper plate	10°-80°
Contact angle of lower plate	90°
Initial distance between two plates	1.5 mm
Initial movement speed of upper plate	1 mm/s
Ink density	1950 kg/m^3
Ink viscosity	9 pa·s
Surface tension of conductive ink	0.03 N/m
Moving distance of upper plate	4.5 mm

In the process of simulating the tensile fracture of the liquid bridge between two plates, the air phase is defined as the first basic item, the conductive silver ink is defined as the second basic item, and it is defined as an incompressible fluid with a volume of 1 μL, which is in contact with the upper and lower plates. Liu [50] verified in experiments that the property of conductive silver ink is pseudoplastic fluid and belongs to laminar flow. Therefore the liquid property in numerical simulation is defined as laminar flow. The upper wall-up of the simulation area is

defined as the pressure outlet, and the left, right, and lower walls are defined as the wall surface [51]. VOF method is used to simulate multiphase flow, Geo-Reconstruct scheme is used to calculate phase volume fraction, and the pressure dispersion solution uses PRESTO!, using the Standard model of Realizable k-ε turbulence model. The dynamic mesh model is adopted, and spring smoothing model and local reconstruction model are selected to update the mesh.

3.3 Comparison of liquid bridge adhesion with theoretical values under different contact angles

The simulation results of liquid bridge adhesion with stretching distance under different contact angles are shown in Table 4. In order to visually express the difference between the simulation results and the theoretical results, a comparison diagram of the changing trend of the two results is drawn. The trend of 10°~40° adhesion with stretching distance is shown in Figure 10 (a), and the trend of 50°~80° adhesion with stretching distance is shown in Figure (b). The comparison results show that the changing trend of liquid bridge adhesion between two plates affected by stretching distance and contact angle obtained by Ansys Fluent numerical simulation software is consistent with the theoretical results, proving that the numerical simulation has high accuracy. There are two reasons for the analysis error: (1) because the mixed grid method is adopted for meshing in numerical simulation, during the upward movement of the structured grid area (fluid-move), the unstructured grid area (fluid) is affected by stretching, and the accuracy at the bottom is not high, and the liquid just adheres with the bottom wall (wall) at this position; (2) In the theoretical derivation part, the liquid volume is approximately replaced by formula (8), and there is an error between the approximate volume and the real volume, which eventually leads to the deviation of the simulation results.

Table 4 Simulation values of adhesion force of liquid bridge under different contact angles

Stretching distance H (mm)	Adhesion force F (x10^{-4}N)							
	10°	20°	30°	40°	50°	60°	70°	80°
0.1	65.21	59.82	55.13	52.14	45.81	33.12	24.41	12.93
0.2	15.13	16.23	14.11	13.03	12.12	9.19	7.00	4.03
0.3	6.87	6.84	6.34	5.92	5.73	4.37	3.40	2.22
0.4	4.17	3.91	3.81	3.63	3.45	2.65	2.26	1.65
0.5	2.54	2.36	2.20	2.43	2.35	1.95	1.63	1.19
0.6	1.57	1.54	1.96	1.62	1.73	1.55	1.25	0.99
0.7	0.97	1.11	1.01	1.22	1.34	1.16	1.00	0.90
0.8	0.51	0.71	0.75	1.00	1.06	1.00	0.86	0.81
0.9	0	0	0.57	0.77	0.86	0.88	0.79	0.75
1.0	0	0	0	0	0	0	0	0

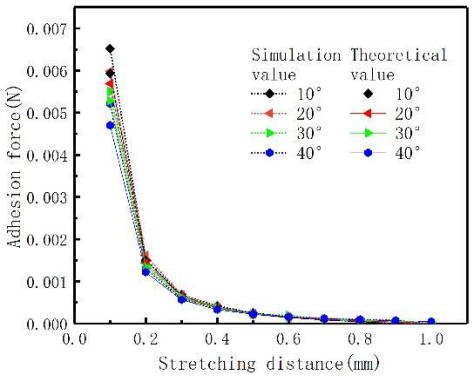

Figure 10 (a) Comparison of simulation value and theoretical value of adhesion force change trend at 10°~40°

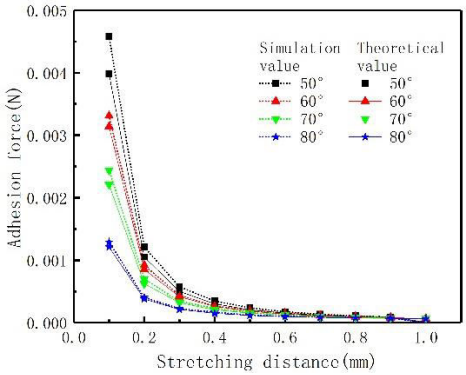

Figure 10 (b) Comparison of simulation value and theoretical value of adhesion force change trend at 50°~80°

3.4 The Relationship Between Liquid Bridge Adhesion and Ink Residue under Different Contact Angles

Conductive ink adheres to the upper plate. When the upper plate moves upwards, the liquid bridge conductive ink is stretched to break. At this time, a part of ink will remain on the surface of the upper plate, which is called residual ink m_{re}. In the two-dimensional numerical simulation, it is assumed that the Z-axis direction is constant per unit length, so the change of contrast conductive ink area can reflect the change of volume. Import the simulation data into CFD-POST software for post-processing, carry out dimensionless treatment on the residual ink, and calculate the percentage of the two-dimensional area S_{ag} of the residual ink on the upper plate to the area $S_{fluid-move}$ of the fluid-move area to obtain the specific amount k_{re} of the proportion of ink residue, as shown in Eq. (18). Furthermore, the changing trend of ink residue under different contact angles was compared.

$$k_{re}=\frac{S_{Ag}}{S_{fluid-move}}\%\,, \tag{18}$$

In order to quantitatively analyze the influence of different contact angles on the residual ink on the upper plate, Figure 11 shows the nephogram of the residual ink when the upper plate stops moving, and the contact angles are 30°, 50°, and 70°, respectively. According to the simulation results, the maximum adhesion of the liquid bridge and the proportion of the residual ink under different contact angles are measured, as shown in Table 5. According to the data in Table 5, the change curves of contact angle, ink residue proportion, and maximum adhesion force are drawn, as shown in Figure 12. It can be seen from the figure that (1) under the premise that the liquid volume between two plates and the contact angle of the lower plate are unchanged, the smaller the contact angle of the upper plate, the greater the amount of ink remaining on the upper plate; (2) Under the same stretching distance (at 0.1mm), the adhesion force of the corresponding liquid bridge increases gradually with the decrease of contact angle. (3) The adhesive force has the same change trend as the residual amount of ink on the upper plate. The reason for this phenomenon is that the contact angle becomes smaller, the ink is easier to spread on the solid surface, the spreading area increases, and the adhesion force correspondingly increases. Compared with the lower plate with an unchanged contact angle, the upper plate will adhere more ink, that is, the residual amount of ink on the upper plate will increase after the liquid bridge between the two plates is stretched and broken.

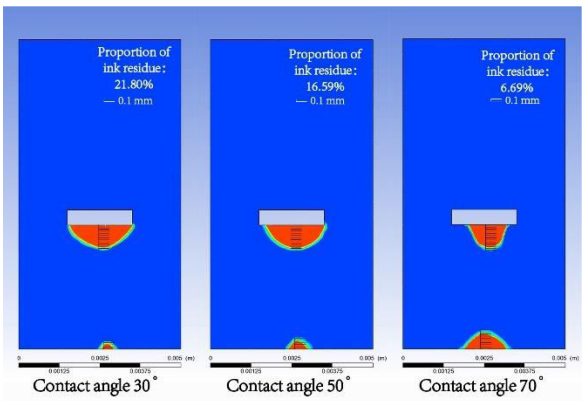

Figure 11 Cloud picture of numerical simulation of ink residue

Table 5 Simulation values under different contact angles

Contact angle of upper plate	Maximum adhesion force F of liquid bridge	Proportion of ink residue
θ/(°)	F/(x10^{-3}N)	k_{re}/(%)
10°	6.52	32.18
20°	5.98	26.51
30°	5.50	21.80
40°	5.21	21.48
50°	4.58	16.59
60°	3.31	7.68
70°	2.44	6.69
80°	1.29	5.05

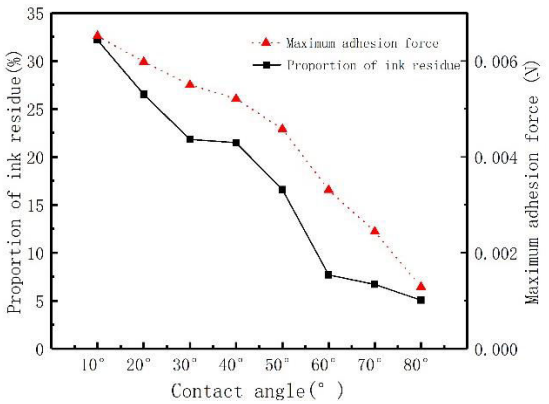

Figure 12 Change trend of ink residue proportion and adhesion under different contact angles

3.5 The Relationship Between Liquid Bridge Adhesion and Stretching Distance under the Same Contact Angle and Different Liquid Volume

Figure 13 shows the nephogram of marked liquid volume before the upper plate moves, which is 0.2V, 0.4V, 0.6V, 0.8V, and 1V respectively, and the initial liquid volume is 1V is 1 μL. Table 6 shows the variation of liquid bridge adhesion and stretching distance under different liquid volumes when the contact angle of the two plates is 40. According to the data in Table 6, the curves of adhesion force with stretching distance under different liquid bridge volumes is shown in Figure 14. It can be seen from the figure that: (1) with the increase of stretching distance, the adhesion of liquid bridge decreases gradually under different liquid volumes; (2) Under the same stretching distance, the larger the volume of liquid, the greater the corresponding adhesive force. The reason for this phenomenon is that under the same stretching distance and solid-liquid contact angle, the larger the liquid volume, the larger the solid-liquid contact area, and the greater the corresponding liquid bridge adhesion. The trend of the simulation results is consistent with that of the theoretical derivation shown in Figure 7. Meanwhile, the change of the solid-liquid adhesion force is observed by changing the liquid volume to affect the liquid-solid spreading area, it is further proved that changing the solid-liquid contact angle

in a modified manner affects the solid-liquid spreading area and ultimately changes the liquid bridge adhesion force.

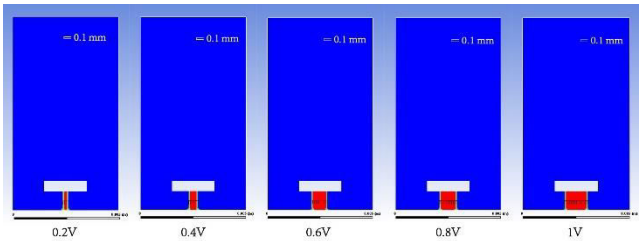

Figure 13　Numerical simulation nephogram of different initial ink volumes

Table 6　Simulation values of liquid bridge adhesion under different liquid bridge volumes

Stretching distance H (mm)	Adhesion force F (x10^{-4}N) Liquid bridge volume(1v=1 μL)				
	0.2v	0.4v	0.6v	0.8v	1v
0.1	12.43	21.23	32.24	38.41	52.11
0.2	2.30	5.56	8.52	10.43	13.24
0.3	0.74	2.94	3.70	4.88	5.92
0.4	0.50	1.63	2.47	3.08	3.63
0.5	0	1.04	1.44	1.96	2.43
0.6	0	0.59	1.00	1.34	1.62
0.7	0	0	0.81	1.01	1.22
0.8	0	0	0.57	0.85	1.00
0.9	0	0	0	0.59	0.77
1.0	0	0	0	0	0

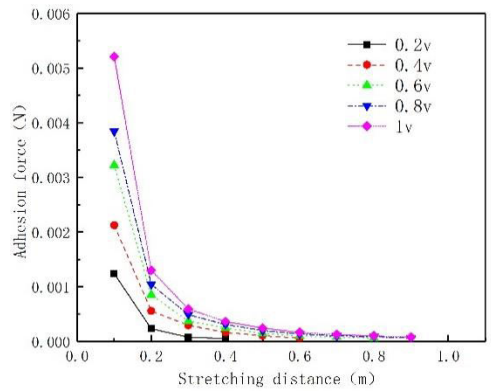

Figure 14　Variation curve of adhesion force with stretching distance under 40° contact angle and different liquid volume

4　Experimental Research

4.1　Experimental Instruments

The liquid bridge tensile test bench developed by the laboratory used in the experiment is shown in figure 15. The contact angle-measuring instrument is DSA100 optical contact angle-measuring instrument produced by KRUSS company in Germany.

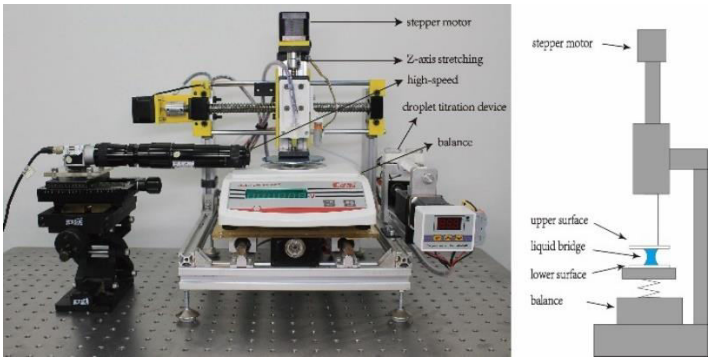

Figure 15　Liquid bridge tensile test bench

4.2 Experimental Materials

The flat materials used in this tensile fracture experiment of the liquid bridge are all 24mm x 50mm glass sheets; The surface treatment agents are NC310 super-hydrophobic solution and NC3082 hydrophilic solution produced by Changzhou Narok Coatings Technology Co., Ltd., and Glaco hydrophobic surface treatment agent produced in Japan, as shown in Figure 16.

Figure 16　Surface treatment agent

4.3　Experimental Scheme Design

Four kinds of glass surfaces with different contact angles were obtained by modifying the glass sheet with three kinds of surface modifiers and leaving the original glass sheet surface unmodified. These four kinds of glass surfaces were used as the upper plate in the tensile fracture experiment of liquid bridge between two plates. By drawing and breaking after adhesion with the ink, the adhesion force of the liquid bridge during static stretching and the amount of ink remaining after the liquid bridge broken were measured.

The measurement of adhesion force during quasi-static stretching of liquid bridge adopts the combination of the liquid bridge stretching test bench and electronic balance to measure the change of adhesion force during stretching of liquid bridge. The measurement method is as follows: fix the unmodified lower plate on the electronic balance, drop a constant volume of conductive silver ink on the lower

plate, and then measure the mass on the electronic balance as m_{down}; when the modified upper plate contacts the ink on the lower plate, measure the mass on the electronic balance as m_{up}. Subtract the two values to obtain the corresponding adhesion force values at different stretching distances in the stretching process, as shown in Eq. (19), where $\boldsymbol{g}$ is the acceleration of gravity. When the liquid bridge is stretched and broken, record the mass m_{la} of the lower plate at this time and find the difference before and after to obtain the mass m_{re} of the ink remaining on the upper plate, as shown in Eq. (20). After dimensionless treatment of ink residue, the ratio of m_{re} to the initial ink quality m_{down} of the lower plate was calculated, and the ink residue ratio $k_{re}^{'}$ was obtained as shown in Eq. (21).

$$F = \left(m_{down} - m_{up}\right) g \,, \tag{19}$$

$$m_{re} = m_{down} - m_{la} \,, \tag{20}$$

$$k_{re}^{'} = \frac{m_{re}}{m_{down}} \% \,, \tag{21}$$

Each group of experiments was repeated 15 times, and the bad values in the measured results of this experiment were removed by the Dixon criterion. Then, the average value of the experimental data was taken, and the results were added to the experimental data analysis table, and finally the modification scheme corresponding to the minimum ink residue was obtained.

4.4 Experimental Results and Discussion

Environmental conditions of this experiment: the ambient temperature of the liquid bridge tensile test bench is (22±1) °C, and the relative humidity of air in the ambient environment is (27±5) %.

4.4.1 Analysis of Theoretical and Experimental Results of Adhesion

Figure 17 shows the contact angle measurement diagram of conductive ink on four different modified surfaces. Respectively use NC3082 modified solution to make the hydrophilic treatment surface, the contact angle is 31.4°; use NC310 modification solution to make the hydrophobic treatment surface, the contact angle is 65.3°; use glaco modification solution to make the hydrophobic treatment surface, the contact angle is 56.4°; the glass surface without any modification treatment has a contact angle of 42.2°.

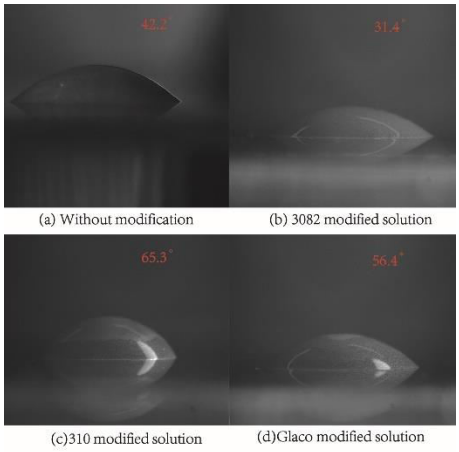

Figure 17 contact angle measurement diagram

The quasi-static liquid bridge tensile fracture experiments were carried out on four different surfaces, and the variation values of adhesion force with stretching distance were obtained by experimental measurement, as shown in Table 7. According to the data in Table 7, the curves of adhesion force with stretching distance on four surfaces were drawn, as shown in Figure 18. It can be seen from the figure that: (1) with the increase of stretching distance, the adhesion force of four different modified surfaces decreases gradually with stretching distance; (2) Under the same stretching distance, the larger the contact angle is, the smaller the corresponding adhesion is; It can also be seen from the figure that the adhesion force and the theoretical and simulation results are quite different. The reasons for this change are as follows: (1) The minimum amount of ink extruded by the ink titration device is 10μL, which exceeds the maximum volume limit without the influence of gravity, so the conductive ink is affected by gravity during stretching, thus affecting the numerical change of adhesion force; (2) In the theoretical part, only capillary force is considered as the main force of adhesion force, and the influence of van der Waals force and electrostatic force are not considered. (3) In the theoretical derivation and numerical simulation of the tensile fracture of the liquid bridge between two plates, it is considered that the moving speed in the vertical direction is far greater than that in the transverse direction, and the transverse speed is neglected. In the actual experiment, the transverse speed has an influence on the ink transfer, which eventually leads to the deviation of the experimental results. However, the overall trend of adhesive force change accords with the conclusion of the theoretical model and numerical simulation, that is, the adhesive force of liquid bridge decreases with the increase of stretching distance, and the adhesive force of liquid bridge decreases with the increase

of contact angle at the same stretching distance.

Table 7 Experimental values of adhesion under different contact surfaces

Stretching distance H/(mm)	Adhesion F (x10^{-2} N) 3082 modified solution θ/(31.4°)	Without modification θ/(42.2°)	Glaco Modified solution θ/(56.4°)	310 modified solution θ/(65.3°)
0.1	7.32	7.21	6.98	6.76
0.2	5.85	5.28	4.32	4.10
0.3	5.68	4.84	4.30	3.66
0.4	5.12	4.42	3.96	3.63
0.5	3.57	2.96	2.71	2.61
0.6	3.21	2.93	2.63	0
0.7	1.42	1.34	0	0
0.8	0	0	0	0
0.9	0	0	0	0
1.0	0	0	0	0

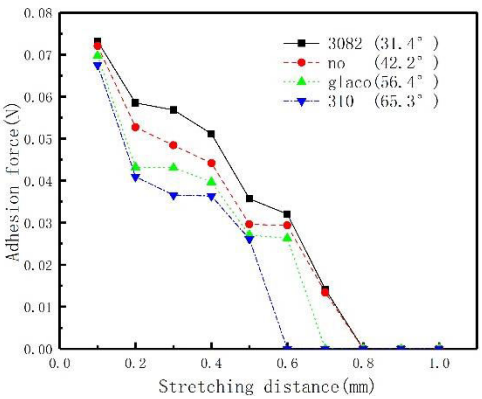

Figure 18 Variation curve of adhesion force with stretching distance of liquid bridge under different contact angles

4.4.2 Analysis of simulation results and experimental results of the residual amount

Quasi-static tensile fracture experiments were carried out on four different surfaces, and the measured values of different contact angles and ink residue ratio are shown in Table 8. According to Table 8, a comparison diagram of the changing trend of ink residue in simulation results is drawn, as shown in Figure 19. It can be found that with the increase of solid-liquid contact angle, the quality of ink remaining on the upper plate decreases. The changing trend is the same as that obtained by simulation results, which proves the accuracy and reliability of numerical simulation.

Table 8 Experimental values of ink residue under different surfaces

	3082 modified solution θ/(31.4°)	Without modification θ/(42.2°)	Glaco modified solution θ/(56.4°)	310 modified solution θ/(65.3°)
Proportion of ink residue k'_{re} /（%）	41.67	33.29	27.78	16.7

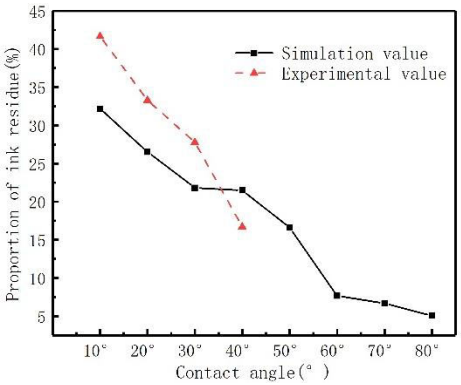

Figure 19 Influence of different contact angles on the proportion of ink residue

5 Conclusions

(1) The classical wetting theory is used to analyze the influence of solid surface energy on the adhesion ability between solid and liquid. Combined with screen printing process, the adhesion model of liquid bridge between two plates is established, and Ansys Fluent is used to simulate the adhesion of liquid bridge. Through model calculation and Ansys Fluent simulation, it can be concluded that contact angle, stretching distance and liquid volume are the main factors affecting the adhesion of liquid bridge. Under the condition of the same stretching distance and liquid volume, the larger the contact angle is, the smaller the adhesion of liquid bridge is.

(2) The fracture of liquid bridge is simulated by Ansys Fluent, and the relationship between adhesion of liquid bridge and ink residue is established. Through liquid bridge fracture simulation and liquid bridge fracture experiment, it can be concluded that the smaller the adhesion between solid and liquid, the smaller the residual amount of liquid on the upper plate after tensile fracture. The numerical simulation results are in good agreement with the theoretical results, which verifies the conclusion of the theoretical model and proves its accuracy.

(3) Based on the adhesion model and the simulation of liquid bridge fracture, the residual rule of conductive

ink on the screen surface was revealed, and verified by the tensile fracture experiment of liquid bridge between two plates on different modified substrates. According to the rule of residual conductive ink on the screen surface, the larger the contact angle is, the smaller the residual conductive ink on the screen surface is. The influence trend of adhesion on residue is the same as that of theoretical model and numerical simulation, which proves the accuracy of theoretical model and numerical simulation, and verifies the rationality of the modification direction proposed in this paper.

7 Declaration

Acknowledgements
Not applicable

Funding
Not applicable

Availability of data and materials
The datasets supporting the conclusions of this article are included within the article.

Authors' contributions
The author' contributions are as follows: Ye Tian wrote the manuscript; Yan Li and Ying-Cai Yuan were responsible for guiding the thesis writing; Lin Zhao was responsible for revising the thesis; Gao-Shen He assisted with experimental platform construction; Tuo-Kai Peng was involved in the theoretical formula derivation; Jian-Lin Xu assisted with sampling and laboratory analyses.

Competing interests
The authors declare no competing financial interests.

Consent for publication
Not applicable

Ethics approval and consent to participate
Not applicable

References

[1] Z Cui. Printed Electronics: New Opportunities in the Traditional Printing Industry. Screen Printing Industry, 2009, 5: 9-11. (in Chinese)

[2] A Martínez-Olmos, J Fernández-Salmerón, N Lopez-Ruiz, et al. Screen printed flexible radiofrequency identification tag for oxygen monitoring. Analytical Chemistry, 2013, 85(22): 11098-11105.

[3] B Peng, X Ren, Z Wang, et al. High performance organic transistor active-matrix driver developed on paper substrate. Rep, 2014, 4: 6430.

[4] B J Carey, J Z Ou, R M Clark, et al, Wafer-scale two-dimensional semiconductors from printed oxide skin of liquid metals. Nature Communications,2017.

[5] K Liu, T T Larsen-Olsen, Y Lin, et al. Roll-coating fabrication of flexible organic solar cells: comparison of fullerene and fullerene-free systems. Journal of Materials Chemistry A, 2016,4.

[6] N Nakayama, H Matsumoto, A Nakano, et al. Screen Printed Thin Film CdS/CdTe Solar Cell. Japanese Journal of Applied Physics, 1980, 19(4): 703-712.

[7] K Kuribayashi, H Matsumoto, H Uda, et al. Preparation of Low Resistance Contact Electrode in Screen Printed CdS/CdTe Solar Cell. Japanese Journal of Applied Physics, 2014, 22(Part 1, No. 12): 1828-1831.

[8] Cheek, G. C, Mertens, et al. Thick-film metallization for solar cell applications. Electron Devices IEEE Transactions on,1984.

[9] H Matsumoto, K Kuribayashi, H Uda, et al. Screen-printed CdS/CdTe solar cell of 12.8% efficiency for an active area of 0.78 cm 2. Solar Cells,1984, 11(4): 367-373.

[10] A Nakano, S Ikegami, H Matsumoto, et al. Long-term reliability of screen printed CdS/CdTe solar-cell modules. Solar cells,1986, 17(2-3): 233-240.

[11] S Ikegami. CdS/CdTe solar cells by the screen-printing-sintering technique: Fabrication, photovoltaic properties and applications. Solar Cells,1988, 23(1-2): 89-105.

[12] R Hokari, K Kurihara, N Takada, et al. Electric characterization of fine wires formed with capillary-effect-based screen-printing. Iet Micro & Nano Letters, 2016, 11(10): 606-610.

[13] K Shetty, Y Kaushal, D S Murthy, et al. Advanced fine line double printing process for manufacturing high efficiency silicon wafer solar cells. Solar Energy, 2019, 180(MAR.): 301-306.

[14] Aakella, P. S., Saravanan, et al. Pre-metallization processes for c-Si solar cells. Solar energy, 97, 388-397.

[15] F C Krebs. Roll-to-roll fabrication of monolithic large-area polymer solar cells free from indium-tin-oxide. Solar Energy Materials & Solar Cells, 2009, 93(9): 1636-1641.

[16] A J Bandodkar, R Nunez-Flores, W Jia, et al. All‐Printed Stretchable Electrochemical Devices. Advanced Materials, 2015, 27(19): 3060-3065.

[17] A Lorenz, M Linse, H Frintrup, et al. Screen printed thick film metallization of silicon solar cells—recent developments and future perspectives. In: 35th European Photovoltaic Solar Energy Conference and Exhibition, 2018. p. 819-824.

[18] D Erath, A Filipovi, M Retzlaff, et al. Advanced screen printing technique for high definition front side metallization of crystalline silicon solar cells. Solar Energy Materials and Solar Cells, 2010, 94(1): 57-61.

[19] Dolden, E. D. (2005). Fundamental investigations into screen printing (Doctoral dissertation, University of Leeds).

[20] W J Hyun, S Lim, B Y Ahn, et al. Screen printing of highly loaded silver inks on plastic substrates using silicon stencils. ACS applied materials & interfaces, 2015, 7 (23): 12619-12624.

[21] Schwanke, D., Pohlner, et al. Enhancement of fine line print resolution due to coating of screen fabrics. Journal of microelectronics and electronic packaging, 6(1), 13-19.

[22] K A Aal, C Yüce, N Willenbacher. Non-Volatile Free Silver Paste Formulation for Front-Side Metallization of Silicon Solar Cells. Solar Energy Materials and Solar Cells, 200, 110040.

[23] S Tepner, N Wengenmeyr, L Ney, et al. Improving wall slip

behavior of silver pastes on screen emulsions for fine line screen printing. Solar Energy Materials and Solar Cells, 2019, 200: 109969.
[24] M R Somalu, A Muchtar, W R W Daud, et al. Screen-printing inks for the fabrication of solid oxide fuel cell films: a review. Renewable and Sustainable Energy Reviews, 2017, 75: 426-439.
[25] Y Tian, Y Li, Y C Yuan, et al. Influence of Screen Printing Electronic Process Parameters on Printing Quality. Packaging Engineering, 2020, 41(05): 250-259. (in Chinese)
[26] K Drabczyk, P Panek. Influence of screen printing parameters on the front metallic electrodes geometry of solar cells. Circuit World,2014.
[27] S P Liu, Y Li, Y Tian, et al. Screen Printing Conductive Ink Transfer Mechanism and Simulation Research. Journal of Mechanical, 2021, 57(5): 231-241. (in Chinese)
[28] T-M Lee, J-H Noh, I Kim, et al. Reliability of gravure offset printing under various printing conditions. Journal of Applied Physics, 2010, 108(10): 102802.
[29] H Y Chu, Z H Chen, L Su, et al. Ink Flow Field and Ink Transferring Rate on Two Ink Rollers. Journal of Beijing University of Technology, 2013, 39(3): 359-365. (in Chinese)
[30] N Kapur, S J Abbott, E D Dolden, et al. Predicting the behavior of screen printing. IEEE Transactions on Components, Packaging and Manufacturing Technology, 2013, 3(3): 508-515.
[31] Y Y Zhang, L Jiang, B Yu, et al. Research Progress on Surface Adhesion Regulation under Dry Environment. Tribology: 1-25. (in Chinese)
[32] S H Kim, D B Asay, M T Dugger. Nanotribology and MEMS. Nano today, 2007, 2(5): 22-29.
[33] W X Yang, X L Wang, P Chen. Optimal Design of Surface Texture in Triboelectric Nanogenerators. Journal of Mechanical, 2020, 56 (03): 130-136. (in Chinese)
[34] W J Zhao, L P Wang, Q J Xue. Development and Research Progress of Surface Texturing on Improving Tribological Performance of Surface. Tribology, 2011, 31 (06): 622-631.
[35] J Q Liu, L F Wang, H L Peng, et al. Dry bonding medical tape and preparation method thereof. CN103654764A. (in Chinese)
[36] Y Huang. Highly switchable and reversible dry adhesion for transfer printing. National Science Review, 2020, 7(03): 558-559.
[37] A Suh, S-C Lee, A Polycarpou. Adhesion and friction evaluation of textured slider surfaces in ultra-low flying head-disk interfaces. Tribology Letters, 2004, 17(4): 739-749.
[38] K Holmberg, A Matthews. Coatings Tribology: properties, mechanisms, techniques and applications in surface engineering Ed. 2. Elsevier Science (2009).
[39] F Buja, G Fiorentino, J Kokorian, et al. Observation of nanoscale adhesion, friction and wear between ALD Al2O3 coated silicon MEMS sidewalls. Nanotechnology, 2015, 26(25): 255701.
[40] J J Ma, W Ou, J B Luo. Wafer-level packaging method based on silicon molecular sieve and polytetrafluoroethylene composite film. CN105236348A (in Chinese)
[41] H Minsky, K T Turner. Composite microposts with high dry adhesion strength. ACS applied materials & interfaces, 2017, 9(21): 18322-18327.
[42] C Wu, X Zhang, H Che, et al. Preparation of nano-convex and nano-concave-patterned polyimide surfaces and their nano-tribological behavior. Nano, 2017, 12(04): 1750049.
[43] S N Ramakrishna, P C Nalam, L Y Clasohm, et al. Study of adhesion and friction properties on a nanoparticle gradient surface: transition from JKR to DMT contact mechanics. Langmuir,2013, 29(1): 175-182.
[44] T Qing, T Shao, S Wen. Micro-friction and adhesion measurements for Si wafer and TiB 2 thin film. Tsinghua Science and Technology, 2007, 12(3): 261-268.
[45] H Liang, Y Bu, Y Zhang, et al. Conversion of organic films into fluorine-containing onion carbon as anti-adhesion solid lubricants. Materials Letters, 2018, 233: 310-313.
[46] D Bonn, J Eggers, J Indekeu, et al. Wetting and spreading. Reviews of modern physics, 2009, 81(2): 739.
[47] T Young. III. An essay on the cohesion of fluids. Philosophical transactions of the royal society of London, 1805(95): 65-87.
[48] K L Mittal, A Pizzi. Adhesion promotion techniques: technological applications. CRC press.
[49] Gennes, Pierre-Gillesde, Brochard-Wyart, et al. Capillarity and wetting phenomena : drops, bubbles, pearls, waves. Springer Science & Business Media.
[50] S P Liu, Y Li, Q L Wang. Analysis and Experiment on Spreading Process of Gravure Printing Electronic Ink. Packaging Engineering, 2019, 40(13): 246-251. (in Chinese)
[51] S Thirumalaikumaran, N Mithran, R Suwathy, et al. A note on using VOF method for polymer bead manufacturing. International Journal of Plastics Technology, 2018, 22(1): 170-176.

Biographical notes

Ye Tian, born in 1995, is currently an engineer at *Beijing Key Laboratory of Digitization Printing Equipment, Beijing Institute of Printing, Beijing*. He received his master degree from *Beijing Institute of Graphic Communication, China*, in 2021. His research interests are screen printing electronics.
E-mail: 787706522@qq.com

Yan Li, born in 1965, is currently an professor at *Beijing Institute of Graphic Communication, China*. She received his master degree from *Beijing University of Aeronautics and Astronautics, China*, in 1999. Her research interests are flexible electronic technology and equipment, printing machinery innovation design, Triz theory and application.
E-mail: 137330424@qq.com

Ying-Cai Yuan, born in 1973, is currently an associate professor at *Beijing Institute of Graphic Communication, China. Zhejiang University, China*. He received his master degree from *Central South University, China*, in 2011. His research interests are flexible electronic technology and equipment and printing machinery innovation design.
E-mail: yuan_yc@bigc.edu.cn

Lin Zhao, born in 1964, is currently a professor at *Shougang CO.,Ltd, China*. He received his PhD degree from *Northeastern University, China,* in 1997. His research interests include mechanics engineering, metal material and automatic control.
E-mail: 13522592591@163.com

Gao-Shen He, born in 1985, is currently an engineer at *Beijing Key Laboratory of Digitization Printing Equipment, Beijing Institute of Printing, Beijing*. He received his master degree from *Beijing Institute of Graphic Communication, China*, in 2021. His research interests include Bio-3D printing, digital printing, medical robotics.

E-mail: 591526804@qq.com

Tuo-Kai Peng, born in 1993, is currently a master candidate at *Beijing Advanced Innovation Center for Soft Matter Science and Engineering*, Beijing University of Chemical Technology, China.
E-mail: PengTuokai@163.com

Jian-Lin Xu, born in 1998, is currently a master candidate at *Beijing Institute of Graphic Communication, China.* His research interests are screen printing electronics.
E-mail: 1770170376@qq.com

Authors' information

1. Beijing Key Laboratory of Digitization Printing Equipment, Beijing Institute of Graphic Communication, Beijing 102600;
2. Research Center of Printing Equipment of Beijing Universities, Beijing Institute of Graphic Communication, Beijing 102600;
3. Beijing Engineering Research Center of Printed Electronics, Beijing 102600;
4. Beijing Shougang Co., Ltd., Beijing 102206;
5. Beijing Advanced Innovation Center for Soft Matter Science and Engineering, Beijing University of Chemical Technology, Beijing 100029